Journal of Materials Chemistry

View Online
Dynamic Article Links

Cite this: J. Mater. Chem., 2011, 21, 12650

www.rsc.org/materials

PAPER

Multifunctional Fe_3O_4 nanoparticles for targeted bi-modal imaging of pancreatic cancer†

Cristina I. Olariu,[a] Humphrey H. P. Yiu,‡[a] Laurent Bouffier,§[a] Taoufik Nedjadi,[b] Eithne Costello,[b] Steve R. Williams,[c] Christopher M. Halloran*[b] and Matthew J. Rosseinsky*[a]

Received 1st April 2011, Accepted 15th June 2011
DOI: 10.1039/c1jm11370d

Amine and carboxylic acid-bifunctionalized iron oxide nanoparticles with robust silane linkages to the nanoparticle surface were prepared with a versatile direct grafting protocol. The contrast in chemistry of these two groups was highlighted by attaching a fluorophore, Rhodamine B isothiocyanate (RITC) onto the amine group and an antibody (EPCAM – epithelial cell adhesion molecule) onto the carboxylic acid groups. The iron oxide core and the RITC tags provide the MRI-fluorescent bi-modal imaging capability. The EPCAM antibody is specific to a protein ubiquitously expressed on the epithelial cell surface. These bifunctionalized nanoparticles target and then undergo facilitated uptake into pancreatic cancer cells (Panc-1) in a time course-monitored controlled study. The integrated optical imaging properties of these magnetic nanoparticles were utilized to monitor the interaction of the nanoparticles with the EPCAM receptors on the cell membrane of the Panc-1 cells. The time-course of the uptake for the targeted and the control particles by the cells was followed allowing the localization within the cell and the impact of particle functionalization to be identified. This system is a candidate for further development as a multi-modular imaging, diagnostic and delivery tool.

Introduction

Pancreatic cancer is a major cause of cancer-related deaths in both the US and Europe.[1,2] Surgery with follow on chemotherapy offers the best chance of survival. However, due to late presentation and diagnosis, this option is not possible for the majority of patients. In order to improve the survival rate of pancreatic cancer, adaptive novel diagnostic techniques are badly needed. Nanomedicine is a rapidly developing field with a myriad of novel nanomaterials of various physical and chemical properties available for scientists as diagnostic and therapeutic research tools including drug delivery agents, molecular recognition agents, gene delivery agents, cancer treatment materials and imaging contrast agents.[3–11] Magnetic nanoparticles (MNPs) are of particular interest for nanomedicine as they can be localized to the target tissue *via* a magnetic field.[12,13] Crucially, however, this is unlikely in itself to achieve greater tissue delivery of cargo, rather than just an accumulation around the site. Thus, if such MNPs are additionally functionalized with specific targeting ligands[14–16] then they have the potential advantage of greater delivery accuracy and facilitated uptake into the site in question. In terms of a chemotherapeutic cargo, this would reduce 'off target' side effects of the drugs on healthy neighboring tissues, which are responsible for a number of unpleasant and serious side effects. Similarly, the ability to image a pathophysiological process at the cellular and molecular level using Magnetic Resonance Imaging (MRI)[17,18] or allied techniques is currently impaired by the lack of specifically targeted contrast agents. MNPs have been widely used as MRI contrast enhancers[19–21] due to their inherent ability to shorten T_2 relaxation time of the surrounding tissue protons. The drawbacks of the existing MRI contrast agents is their application in the detection of liver or spleen tumours which is based on the uptake of the MNPs by the cells of the mononuclear phagocyte system (passive targeting).[22,23] Development of specific contrast agents for all imaging modalities (MRI, Computerized Tomography

[a]*Department of Chemistry, University of Liverpool, Crown St, Liverpool, L69 7ZD, United Kingdom. E-mail: m.j.rosseinsky@liverpool.ac.uk; Fax: +44-151-794-3589; Tel: +44-151-794-2297*
[b]*Department of Molecular and Clinical Cancer Medicine, 5th Floor UCD Building, Royal Liverpool University Hospital, Daulby St, Liverpool, L69 3GA, United Kingdom. E-mail: halloran@liverpool.ac.uk; Fax: +44-151-706-5798; Tel: +44-151-706 -4087*
[c]*Imaging, Proteomics and Genomics Research Group, University of Manchester, Oxford Road, Manchester, M13 9PT, United Kingdom*

† Electronic supplementary information (ESI) available: TG analysis on **Fe_3O_4-NH_2** and **Fe_3O_4-NH_2/COOH**, TEM and DLS nanoparticles size distribution on Fe_3O_4 and **Fe_3O_4-NH_2/COOH**, **Fe_3O_4-NH-RITC/COOH** Schematic of RITC blocking of remaining NH_2 groups, immunofluorescence labeling of EPCAM expression on Panc-1 cells, antibody concentration measured by Bradford assay and matched to a standard curve. See DOI: 10.1039/c1jm11370d

‡ Current address: Chemical Engineering, School of Engineering and Physical Sciences, Heriot-Watt University, Edinburgh, EH14 4AS, United Kingdom

§ Current address: Univ. Bordeaux, ISM, CNRS UMR 5255, F-33400, Talence, France

(CT) and Positron Emission Tomography (PET)) targeted to tissue/tumours would be central in resolving diagnostic dilemmas.

The key element for the attachment of desired targeting molecules onto MNPs lies on the surface modification with suitable organic functionalities. This can be achieved *via*: polymer coating,[24] surfactant adsorption[12] and direct grafting of organo-silanes.[25] A number of synthetic polymers such as PEG-poly(ethylene glycol),[26] poly(acrylamide)[27] and PVA-poly(vinyl alcohol)[28] as well as naturally occurring polymers such as dextran[29] and chitosan[30] have been used to modify the surface properties of the MNPs for enhancing their colloidal stability, biocompatibility and low protein interaction. However, these polymers physisorbed onto the surface of nanoparticles by electrostatic attraction or hydrogen-bonding have shown limited stability because the polymer is likely to detach from the magnetic core under the physiological environment in time.[31] Additionally, modification using polymers reduces the overall magnetic response of MNPs due to the decrease in total iron content.[32] An alternative route to modify the surface of MNPs is to use small molecules such as functional silanes. The direct silanization of the surface of MNPs forms a robust, covalent coating with grafted functional groups on the surface. This allows further functionalization on the primary functional groups to generate a wide variety of surface functionalities to suit specific applications.[33–35] 3-Aminopropyltriethoxysilane (APTES) is commonly used to prepare cationic amine groups on MNPs.[36] This system offers only one functional group for chemical conjugation with targeting ligands or fluorescent tags. However, if a second functionality is attached (for example carboxylic groups), it is advantageous for covalent conjugation with targeting ligands and fluorescent molecules simultaneously.

Fluorescent iron oxide nanoparticles tagged with antibodies for targeted imaging have been reported in recent years.[37–42] Several of these adopted the polymer coating strategy. For example, Yang *et al.*[40] reported a magnetic-fluorescent nanohybrid with Cetuximab antibody for targeting human epithelial cancer cells while Zou *et al.*[41] demonstrated a system with PEG-coated SPION with both 5-AM fluorescent label and HuCC49ΔCH2 antibody for targeting colon cancer cells. Another system reported by Makhluf *et al.*[42] used PVA-coated Fe_3O_4 nanoparticles with an anti-protein kinase C (PKC) alpha antibody and a fluorescent tag for targeted imaging of sperm cells. However, in these cases, the functionalities are grafted onto the polymer shell which causes an increase in the overall size of nanoparticles. A polymer-free, bifunctional magnetic nanoparticle system covalently tagged with fluorescent molecules and antibodies is demonstrated here.

In this work, we use a simple direct-grafting synthetic pathway for preparing Fe_3O_4 nanoparticles with both amine (NH_2) and carboxyl (COOH) functionalities co-existing in one nanoparticle. The fluorescent molecules are covalently attached to the amine groups while the carboxylic functional groups allow chemical coupling with targeting ligands. This allows cancer-specific targeting and has dual-imaging capability (fluorescent and MRI) with low toxicity. The ability of these multifunctional nanoparticles (with an antibody specific for epithelia) to localize and allow facilitated uptake into a pancreatic cancer cell line (Panc-1) has been demonstrated in a controlled time-course study. With the addition of distinct fluorophores and active targeting elements this single nanoparticle platform would offer potential for the progress of cancer diagnosis and treatment.

Results and discussion

Formation of dual functional groups on the surface of Fe_3O_4 nanoparticles

Silanization with organofunctional alkoxysilane molecules was used to functionalize the surface of 25 nm MNPs, following a modified procedure described in the literature.[36] The first step is to prepare an amine-functionalized MNP (Fig. 1a), sample denoted **Fe_3O_4-NH_2**, by grafting APTES onto the surface of commercial 25 nm Fe_3O_4 nanoparticles. The presence of amine groups on **Fe_3O_4-NH_2** was qualitatively monitored by Fourier transform infrared spectroscopy (FTIR). Fig. 2a indicates the successful grafting of silane molecules evidenced by the presence of the two broad bands at 3435 and 1600 cm^{-1} in the FTIR spectrum of **Fe_3O_4-NH_2**, which were assigned to the N–H stretching vibration and N–H bending respectively.[43] The peaks observed at 2925 and 2850 cm^{-1} are due to the symmetric and the asymmetric CH_2 stretching modes respectively.[44] Fe–O–Si bonds are masked in the FTIR spectrum by overlapping with the Fe–O vibrations of magnetite at 580 cm^{-1}.[45] On the other hand, formation of the silane layer on the surface of nanoparticles was confirmed by the band at 1118 cm^{-1} corresponding to the Si–O–Si bond.[46]

Quantitative analyses on the composition of the **Fe_3O_4-NH_2** nanoparticles were carried out using CHN elemental analysis and thermogravimetric analysis (TGA), in order to estimate the number of amine functional groups grafted on the surface. The carbon content of carefully isolated functional nanoparticles increased from 0.08% C in unfunctionalized nanoparticles

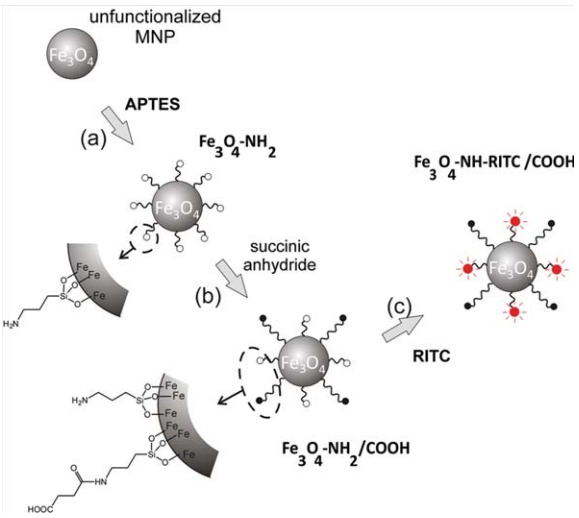

Fig. 1 Iron oxide MNPs functionalization. (a) APTES, toluene, 110 °C, overnight to produce amine functionalized nanoparticles denoted as **Fe_3O_4-NH_2**; (b) succinic anhydride, dimethylformamide, room temperature, 24 h to produce bifunctionalized nanoparticles denoted as **Fe_3O_4-NH_2/COOH**; (c) RITC, sodium bicarbonate buffer, room temperature, overnight to produce fluorescently labelled nanoparticles denoted as **Fe_3O_4-NH-RITC/COOH**.

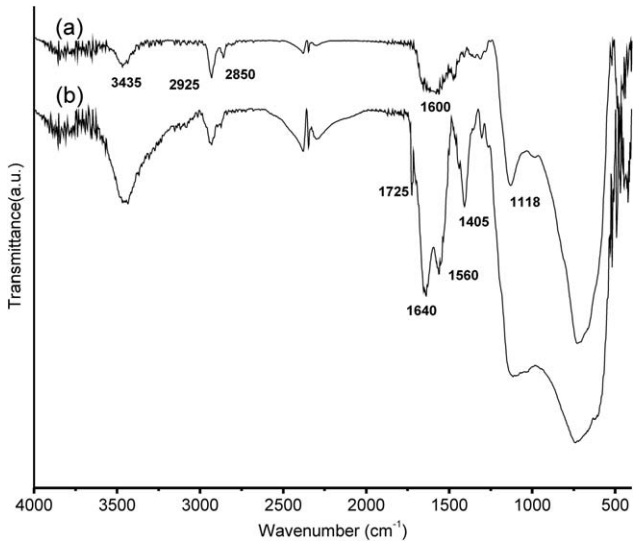

Fig. 2 FTIR spectra recorded between 4000 and 400 cm^{-1} of functionalized magnetic nanoparticles: **Fe_3O_4-NH_2** (a) shows the presence of the NH_2 groups by the bands at 3435 and 1600 cm^{-1}; **Fe_3O_4-NH_2/COOH** (b) confirms the free carboxylic groups by the band at 1725 cm^{-1}.

(assigned to surface sorption of CO_2) to 1.22% C in **Fe_3O_4-NH_2**. From the increased carbon content, there is an estimated 0.34 mmol of silane ligands per gram of nanoparticles and the composition for **Fe_3O_4-NH_2** is $(Fe_3O_4)_{13}(O_3SiC_3H_8N)_1(H_2O)_1$. Based on the average diameter of a spherical particle being 25 nm (from TEM analysis) and the density of Fe_3O_4 being 5.17 g cm^{-3}, an average number of 8600 amine molecules can be estimated on top of each nanoparticle (or 4.38 silane ligands nm^{-2}, a distance around 0.3 nm between two NH_2 groups). This result is in agreement with previous reports regarding the density of silane ligands on nanoparticles.[47,48] The results are summarized in Table 1. The TGA thermogram of **Fe_3O_4-NH_2** in air (SI, Figure S1†) shows two plateaus. The first between 30 and 150 °C was due to the evaporation of physically absorbed moisture on the surface. This comprises 0.61% weight loss which is consistent with the CHN water content of 0.56%. The second plateau (between 150 and 600 °C) corresponded to the decomposition of propylamine groups. A similar temperature range was also reported for aminosilane-coated cobalt ferrite nanoparticles.[48] TGA was also used to estimate the number of silane ligands anchored on the MNPs according to the following formula: $N = \omega N_A \rho V / MW$, where N is the number of ligands on each nanoparticle, ω is the mass loss in percent, N_A is Avogadro's number, ρ is the density if the nanoparticle, V is the volume of one nanoparticle and MW is the molar weight of the ligands. The weight loss of the **Fe_3O_4-NH_2** recorded by TGA is 2.03% between 150 and 600 °C (SI, Figure S1†) which leads to approximately 8750 amine groups per nanoparticle. This number is consistent with the number of groups based on the CHN data.

In the second synthetic step, carboxylic functional groups were tethered by reacting the surface-bound amine groups with succinic anhydride, resulting in the sample denoted as **Fe_3O_4-NH_2/COOH** (Fig. 1b). The post-functionalization reaction for introducing free carboxylic groups was qualitatively monitored by FTIR. Fig. 2b shows that the free carboxylic groups are present as evidenced by the characteristic C=O stretching absorption at 1725 cm^{-1} in the spectrum of **Fe_3O_4-NH_2/COOH**.[44] Also the frequencies in the region of 1640 cm^{-1} and 1560 cm^{-1} were assigned to the C=O stretching band and N–H bending band in the amide linkage, respectively.[44] The size of MNPs before and after the surface modification with amine and carboxyl groups was examined using transmission electron microscopy (TEM) and dynamic light scattering (DLS). The diameter of the commercial Fe_3O_4 MNPs was found to be 25 ± 5 nm from TEM (Figure S2a†) while their average hydrodynamic size is 164 ± 6 nm from DLS (Figure S2c†). The chemical modification with APTES and succinic anhydride did not change the particle size. The size for **Fe_3O_4-NH_2/COOH** is 24 ± 4 nm from TEM (Figure S2b†) and the average hydrodynamic diameter is 142 ± 8 nm (Figure S2d†). DLS size is larger since it measures the hydrodynamic size of the core surrounded by the solvation layers. Additionally DLS is more accurate for soft materials such as polymers or proteins and the size of more dense materials may be overestimated.[49] The organic compositions of post-functionalized **Fe_3O_4-NH_2/COOH** nanoparticles were also quantified using CHN elemental analysis and TGA. From the elemental analysis, based on the carbon content increase (1.62% C in **Fe_3O_4-NH_2/COOH**), there is an estimated 0.09 mmoles of carboxylic groups per gram of nanoparticles (corresponding to approximately 2300 carboxylic acid groups per NP). The composition for **Fe_3O_4-NH_2/COOH** is $(Fe_3O_4)_{13}(O_3SiC_3H_8N)_{0.75}(O_3SiC_7H_{12}NO_3)_{0.25}(H_2O)_1$. The deconvolution of the TGA data (SI, Figure S1) for **Fe_3O_4-NH_2/COOH** (3.08%–2.03% = 1.05% between 150 and 600 °C) allows estimation of the number of carboxylic acid groups as approximately 2300 per NP (Table 1), which is consistent with the result from CHN elemental analysis. These values correspond to only 25% of post-functionalization but such incomplete conversion in the reaction with succinic anhydride is likely to be due to steric hindrance, heterogeneous phase conditions (solid/liquid) and protonation or lack of nucleophilicity of some amine groups. Such partial conversion of the amine groups to carboxylic acids offers the bifunctionality on the surface of nanoparticles, with 75% free amine groups and 25% carboxylic acid groups. The **Fe_3O_4-NH_2/**

Table 1 Quantitative estimation of the number of amine, carboxylic and RITC groups per nanoparticle based on the carbon content from elemental analysis and the weight loss from TGA (air, 600 °C)

Sample	CHN analysis (C %)	TGA weight loss (%)	Number of functional groups/NP (CHN)	Number of functional groups/NP (TGA)
Fe_3O_4-NH_2	1.22	2.03	8600	8750
Fe_3O_4-NH_2/COOH	1.62	3.08	2300	2300
Fe_3O_4-NH-RITC/COOH	3.63	-	2000	-

COOH nanoparticles are advantageous for tagging two types of functional species reacting with the two distinct $-NH_2$ and –COOH functionalities silane-bound to the NP surface (Fig. 1b). Here we demonstrate this concept by using these groups to attach two species, fluorescent molecules and specific proteins, on a single particle through two different binding chemical strategies. Amine groups were coupled with RITC (Fig. 1c) while carboxyl groups were conjugated with proteins using the carbodiimide coupling (EDC, *N*-(3-Dimethylaminopropyl)-*N*′-ethylcarbodiimide, was used as reagent). EDC was chosen because unlike other cross-linking agents (such as glutaraldehyde) it does not become part of the final nanoparticle-biomolecule cross-link. Also, nanoparticle–nanoparticle and protein–protein crosslinking are not avoidable using glutaraldehyde as a crosslinking reagent.

Rhodamine-tagged bifunctional Fe_3O_4 nanoparticles

Rhodamine B isothiocyanate (RITC) is a commonly used fluorescent tag for biological samples which shows an orange-red emission wavelength (λ_{ex} = 570 nm, λ_{em} = 595 nm). Similar to other isothiocyanate modified fluorophores, RITC is reactive only towards the free amine groups ($-NH_2$) present in the lysine units of peptides and proteins. Since only mild reaction conditions (room temperature, a buffer solution, pH = 9.5) are required for the binding of RITC with an amine group, the **Fe_3O_4-NH_2/COOH** nanoparticles are unlikely to be destabilized and the carboxyl functionalities are to be preserved. In Fig. 3a the fluorescent image of RITC-tagged nanoparticles, denoted as **Fe_3O_4-NH-RITC/COOH**, is shown with clear red fluorescence, which indicates the RITC molecules coupled to the nanoparticles. The amount of RITC bound to the nanoparticles can also be quantified using CHN elemental analysis (Table 1). After the RITC binding the carbon content increased from 1.62% to 3.63% which corresponds to approximately 2000 RITC molecules per nanoparticle and is equivalent to approximately 30% binding of the residual 75% free amine groups after carboxylic acid functionalization. A 30% yield is reasonable considering that the grafted $-NH_2$ groups are rather close to each other (~0.3 nm between groups) while the width of a rigid RITC molecule is around 1.0 nm (measured with ChemBio3D Ultra 12.0 software). As shown in Figure S3,† the two neighboring $-NH_2$ groups to the RITC are likely to be blocked for further reactions. Also the hydrodynamic size of the **Fe_3O_4-NH-RITC/COOH** was measured to be 154 ± 6 nm which is comparable with that of the bifunctionalized nanoparticles and shows no evidence for large aggregation (SI, Figure S2e†). The tagged RITC molecules have two functions: first, their fluorescent property allows traceability of the MNPs using fluorescence imaging; second, RITC molecules can block the residual amine groups and prevent them from reacting with the carboxyl groups in presence of the EDC coupling reagent during protein/antibody coupling. This is particularly important as the same chemistry is used for the binding of proteins and antibodies onto the carboxyl-functionalized Fe_3O_4 nanoparticles. Without the RITC units, crosslinking of nanoparticles might occur, through the binding between the two functionalities (–COOH and $-NH_2$) on surface, during antibody coupling.

In order to confirm that the carboxyl functional groups are still chemically accessible on the **Fe_3O_4-NH-RITC/COOH**, a fluorescent protein, bovine serum albumin tagged with fluorescein isothiocyante or FITC-BSA (FITC λ_{ex} = 488 nm, λ_{em} = 530 nm), was used as a testing reagent. The fluorescent protein was attached by conjugating the carboxyl groups of the nanoparticles with the amine groups on the BSA surface using the EDC coupling method. Since FITC-BSA shows green fluorescence, **Fe_3O_4-NH-RITC/COOH** nanoparticles bound with this fluorescent protein will show both red and green fluorescence. In Fig. 3a the red and green fluorescence is observed on the nanoparticles depicted with a bright field image and this indicates that the fluorescent protein has been successfully tagged onto the red-fluorescent **Fe_3O_4-NH-RITC/COOH** nanoparticles, in turn demonstrating the accessibility of the succinic anhydride-derived carboxyl groups for bioconjugation.

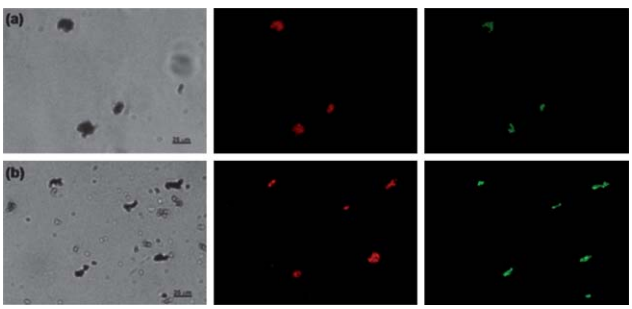

Fig. 3 Bright field and fluorescence microscopy images of (a) **Fe_3O_4-NH-RITC/COOH** conjugated with FITC-BSA: the red fluorescence shows that the RITC fluorescent dye is tagged to the nanoparticles and the green fluorescence shows the FITC-BSA bound to the nanoparticles; (b) **Fe_3O_4-NH-RITC/COOH** conjugated with FITC-IgG: red fluorescence shows that the RITC is tagged to the nanoparticles and the green fluorescence shows that the FITC-IgG is also bound to the nanoparticles. Scale bar: 25 μm.

Antibody-tagged Fe_3O_4 nanoparticles

In the next step, **Fe_3O_4-NH-RITC/COOH** nanoparticles were decorated with a generic antibody molecule tagged with a green fluorescent dye (FITC-IgG). FITC-IgG was chosen as a model antibody because it is commercially available and the binding chemistry for antibodies is applicable to all proteins.[50] The active carboxylic groups on **Fe_3O_4-NH-RITC/COOH** were covalently conjugated with the amine groups on the antibody *via* the carbodiimide method.[50] Fluorescence imaging was used to show that the FITC-IgG molecules were attached to the **Fe_3O_4-NH-RITC/COOH** nanoparticles (Fig. 3b).

The green and red fluorescence are observed on the nanoparticles, as shown in the bright field image. This indicates that FITC-IgG was successfully bound to the red-fluorescent **Fe_3O_4-NH-RITC/COOH** nanoparticles. As a result, specific antibodies can be attached onto the **Fe_3O_4-NH-RITC/COOH** samples with the same coupling protocol as for FITC-IgG or any other proteins.

Evaluation of the effect of functionalized nanoparticles on the magnetic resonance transverse relaxation rate

We assessed whether the functionalized nanoparticles are behaving as contrast enhancers by measuring the transverse

relaxation time T_2, on a 7 T MRI scanner. Measurements were performed at room temperature for iron concentrations between 0.01 and 0.2 mM. Their efficiency as MRI contrast agents was determined by calculation of the r_2 relaxivities as the linear fit of the inverse relaxation times as a function of iron concentration. As seen on Fig. 4a, the signals intensity of T_2 weighted images changed with the increase in Fe concentration. Also, Fig. 4b shows the relaxation rates $1/T_2$ against the different iron concentrations. As expected, the relaxation rates vary linearly with the iron concentration. The relaxivities (equivalent to the slopes of the lines) were found to be 147.8, 149.9, 182.1 and 199 $mM^{-1}s^{-1}$ for Fe_3O_4, **Fe_3O_4-NH_2**, **Fe_3O_4-NH_2/COOH** and **Fe_3O_4-NH-RITC/COOH** respectively. A direct comparison with commercially available magnetic nanoparticles would not be straightforward since the measurements would be performed with different experimental parameters such as field strength. However, our measurements show that the functionalized nanoparticles could be employed as potential MRI contrast agents and that the functionalization does not hinder the contrasting properties.

Cytotoxicity of functionalized Fe_3O_4 nanoparticles

In order to determine whether the **Fe_3O_4-NH_2/COOH** nanoparticles can demonstrate potential for use in biological systems (both *in vitro* and *in vivo*), their cytotoxicity in a human pancreatic cancer cell line (Panc-1), which is also used for the targeting experiments, was evaluated using the MTS cell proliferation assay.[51,52] This is a colorimetric assay which measures a cells enzymatic ability to reduce 3-(4,5-dimethylthiazol-2-yl)-5-(3-carboxymethoxyphenyl)-2-(4-sulfophenyl)-2*H*-tetrazolium (MTS) to formazan dyes, giving rise to an orange colour; hence greater absorbance equates to a greater estimation of cell viability. Monolayers of Panc-1 pancreatic cancer cell lines were grown and then loaded with increasing concentrations of magnetic nanoparticles ranging from 25 to 200 μg mL^{-1}. Control experiments consisting of untreated cells without addition of nanoparticles were used for comparison. The results for unfunctionalized Fe_3O_4 and **Fe_3O_4-NH_2/COOH** nanoparticles showed that the viability of cells was not affected by the presence of the nanoparticles at a level $\leq$ 125 μg mL^{-1} after 48 h of treatment; no statistical significance was observed (non-significant [NS] $p>0.05$) (Fig. 5).

At concentrations of nanoparticles higher than 125 μg mL^{-1} statistically significant decreases in absorbance were seen. Although this was entirely compatible with a decrease in viability of those cells, it cannot be excluded that this was due to cytostasis of the cells caused by the engulfed particles as Fe_3O_4 nanoparticles are reported to be non-toxic for concentrations up to 250 μg mL^{-1}.[53] However, more importantly is the finding that **Fe_3O_4-NH_2/COOH** nanoparticles did not cause any additional toxic effect over and above that of Fe_3O_4. Other papers have also reported that coated iron oxide nanoparticles have good biocompatibility not only *in vitro* but also *in vivo* and that the cytotoxicity effect is dependent on dose, compositions and

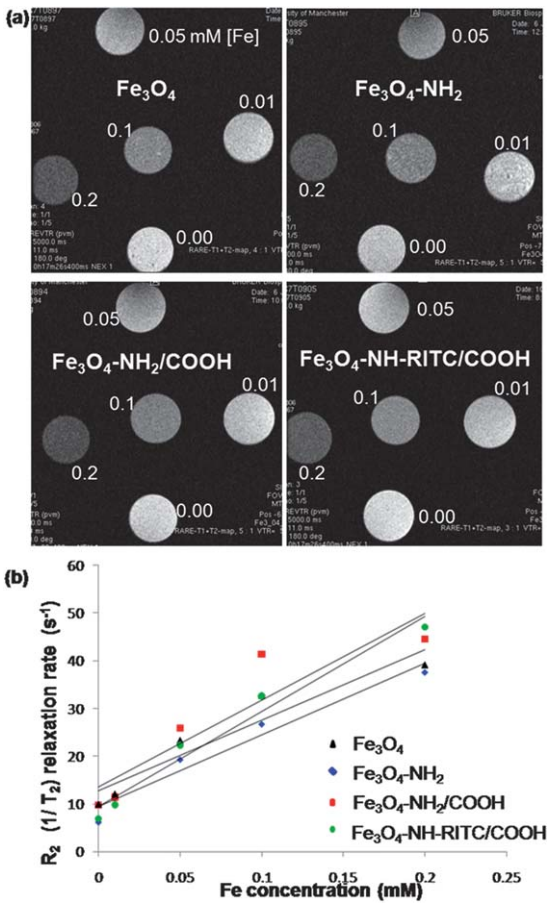

Fig. 4 (a) Moderately T_2 weighted (TE/TR 11/5000 ms) MR images of unfunctionalized Fe_3O_4; **Fe_3O_4-NH_2**; **Fe_3O_4-NH_2/COOH** and **Fe_3O_4-NH-RITC/COOH** and (b) T_2 relaxation rates plotted as function of Fe concentration.

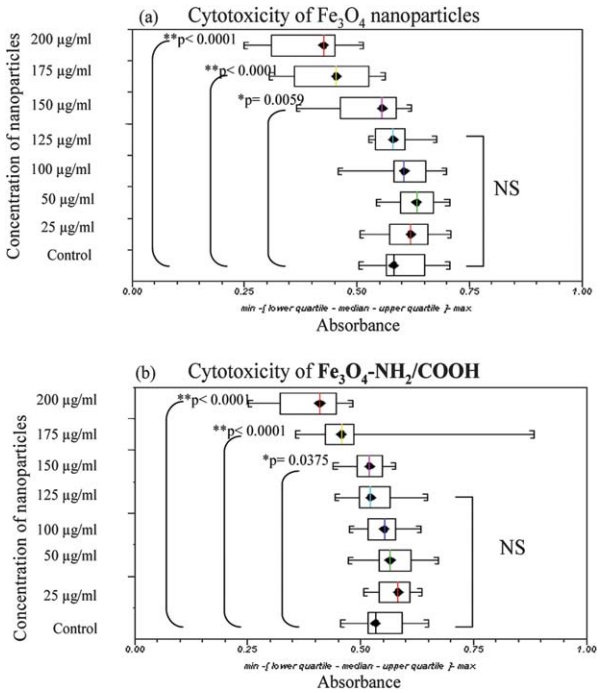

Fig. 5 Cytotoxicity of Panc-1 cells when incubated with different concentrations of (a) unfunctionalized Fe_3O_4 and (b) **Fe_3O_4-NH_2/COOH** for 48 h. Statistical differences between control and samples are reported as: *$p<0.05$, **$p<0.0001$ and NS ($p>0.05$) using the Mann-Whitney U test. n = 3 cultures.

particle size.[53–55] In addition to these findings, our study on cytotoxicity of the bifunctionalized nanoparticles with Panc-1 cells also shows that the newly modified bi-functional surface does not induce any toxicity. For the cell targeting experiments, concentrations of 100 μg mL^{-1} were used, and at this concentration, our analysis showed that the nanoparticles are not cytotoxic/cytostatic when compared with the controls.

Targeting pancreatic cancer cells

For targeting experiments the bifunctional surface of **Fe_3O_4-NH-RITC/COOH** nanoparticles was exploited by adding an additional tag to focus the particle to the cell surface (in this case Panc-1 human pancreatic cancer cell lines). An antibody to a protein ubiquitously expressed on epithelial cell surfaces (epithelial cell adhesion molecule, EPCAM) and known to be highly expressed on Panc-1 cells[56] (SI, Figure S4†) was chosen to prove the principle of antibody-mediated localization of the particles as pictured in Fig. 6.

These nanoparticles were denoted **Fe_3O_4-NH-RITC/CO-EPCAM**. After conjugation, the content of immobilized EPCAM was calculated to be 7.03 μg mg^{-1} nanoparticles (SI, Figure S5†) which correspond to approximately 1.35 molecules EPCAM per MNP. To test the antibody-mediated localization hypothesis, the **Fe_3O_4-NH-RITC/CO-EPCAM** nanoparticles and two negative controls were used in these experiments: Control 1: fluorescent-labelled nanoparticles tagged with a non-specific isotype antibody (which has no specificity for the cells receptors but with all the other characteristics of the antibodies used in the experiment—a negative result would indicate that the bound antibody per se has no role in targeting/uptake), named **Fe_3O_4-NH-RITC/CO-ISO** and Control 2: **Fe_3O_4-NH-RITC/COOH** antibody-free nanoparticles. These were chosen so as to highlight the specificity of **Fe_3O_4-NH-RITC/CO-EPCAM** nanoparticles, such that these particles should be preferentially bound to Panc-1 cells, while **Fe_3O_4-NH-RITC/CO-ISO** and **Fe_3O_4-NH-RITC/COOH** should not. Monolayers of Panc-1 cell lines were separately incubated with these three nanoparticle samples for 1, 6 and 24 h. The ability of the particles to localize the cells was examined using fluorescence microscopy.

In Fig. 7a, in the first hour red fluorescence (from the bound RITC) was only observed from the Panc-1 cells incubated with

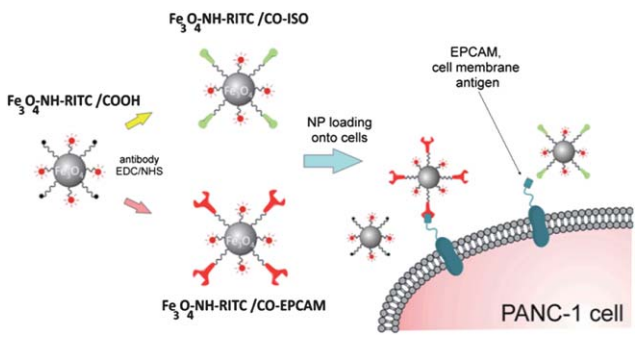

Fig. 6 Schematic illustration of the concept of antibody targeting with Panc-1 cancer cells. **Fe_3O_4-NH-RITC/COOH** nanoparticles were tagged with specific EPCAM antibodies (nanoparticles denoted as **Fe_3O_4-NH-RITC/CO-EPCAM**) or with non-specific isotype antibodies (nanoparticles denoted as **Fe_3O_4-NH-RITC/CO-ISO**).

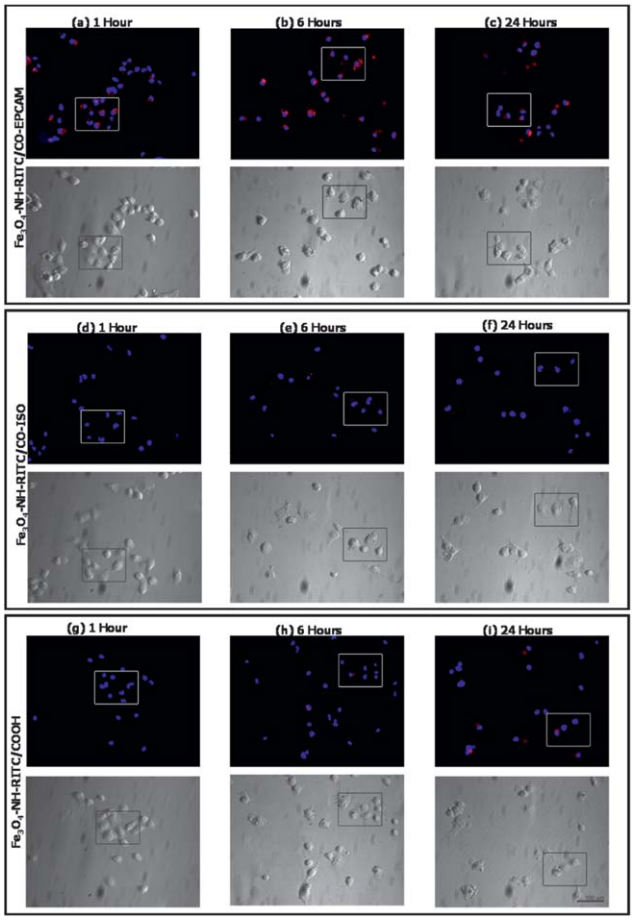

Fig. 7 Fluorescence microscopy images showing the effect of EPCAM modification on targeting abilities of nanoparticles (red fluorescence). The cell nuclei were stained with DAPI (blue fluorescence). First panel: Panc-1 incubated with **Fe_3O_4-NH-RITC/CO-EPCAM** for different timelines (a) 1 h; (b) 6 h and (c) 24 h. Second panel: Panc-1 incubated with **Fe_3O_4-NH-RITC/CO-ISO** for different timelines (d) 1 h; (e) 6 h and (f) 24 h. Third panel: Panc-1 incubated with **Fe_3O_4-NH-RITC/COOH** for different timelines (g) 1 h; (h) 6 h and (i) 24 h. Scale bar 100 μm. Zoom-in images of the highlighted regions (in rectangles) are shown in Figure 7.

Fe_3O_4-NH-RITC/CO-EPCAM. Blue fluorescence is due to the cell nuclei stained with 4′,6-diamidino-2-phenylindole (DAPI) for localization of the cells. This implies targeting of these particles to Panc-1 cells, which has been mediated by surface-to-surface antibody–antigen interactions. Red fluorescence was not observed from the cells incubated with the two controls **Fe_3O_4-NH-RITC/CO-ISO** or **Fe_3O_4-NH-RITC/COOH** nanoparticles in the first hour (Fig. 7d and 7g). The addition of the non- specific antibody (ISO) did not enhance the cellular uptake of nanoparticles due to the fact that this antibody does not present the same specific antigen binding region as EPCAM. Therefore the ISO antibody could not target the nanoparticles to the cell surface, ruling out the non-specific interaction and uptake.

Fig. 8 shows more detailed cell images of Fig. 7 of the zoomed-in areas. For cells incubated with **Fe_3O_4-NH-RITC/CO-EPCAM** nanoparticles, some red fluorescence, likely to be aggregates of **Fe_3O_4-NH-RITC/CO-EPCAM** nanoparticles, was observed near the nuclei (stained with DAPI in blue) while some red particles are localized on the cell membranes (indicated with

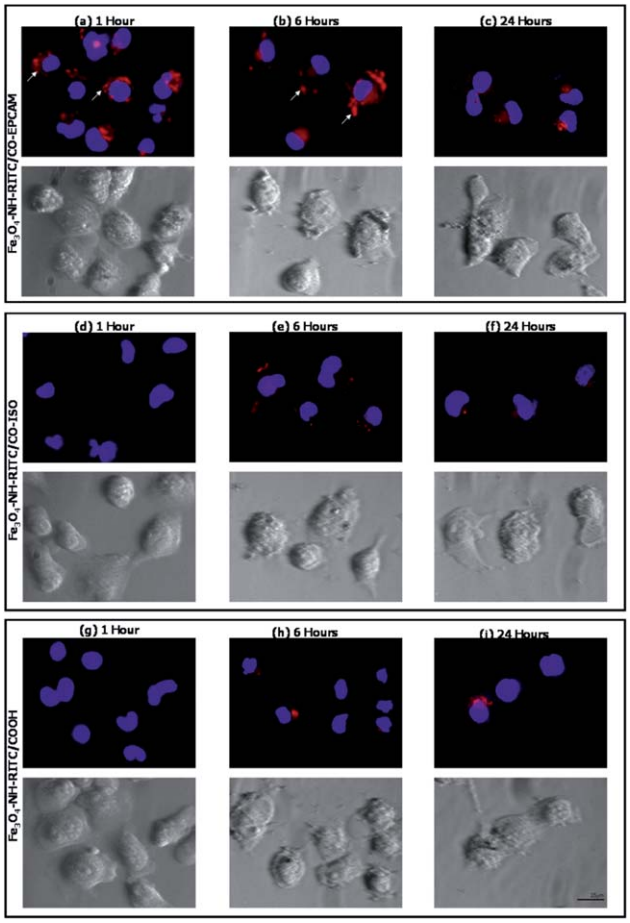

Fig. 8 Magnified fluorescence images of insets in Fig. 6, showing the effect of EPCAM modification on targeting abilities of nanoparticles (red fluorescence). The cell nuclei were stained with DAPI (blue fluorescence). First panel: Panc-1 incubated with **Fe_3O_4-NH-RITC/CO-EPCAM** for different timelines (a) 1 h; (b) 6 h and (c) 24 h. Second panel: Panc-1 incubated with **Fe_3O_4-NH-RITC/CO-ISO** for different timelines (d) 1 h; (e) 6 h and (f) 24 h. Third panel: Panc-1 incubated with **Fe_3O_4-NH-RITC/COOH** for different timelines (g) 1 h; (h) 6 h and (i) 24 h. Scale bar 25 μm.

white arrows in Fig. 8a). This suggested that the internalization of **Fe_3O_4-NH-RITC/CO-EPCAM** nanoparticles occurs within an hour. This was verified by examining sections of similarly treated Panc-1 cells by confocal microscopy. Fig. 9a shows middle section confocal images of Panc-1 with a zoom-in area (Fig. 9b) to confirm that **Fe_3O_4-NH-RITC/CO-EPCAM** nanoparticles accumulated in the cells. It is proposed that these nanoparticles were internalized *via* a receptor mediated endocytosis facilitated by the successful binding onto the EPCAM receptors on cell membranes.

Interestingly at 6 h Panc-1 cells incubated with the controls also show some red fluorescence with intensity increasing at 24 h; although this was substantially less intense than in the case of the cells incubated with **Fe_3O_4-NH-RITC/CO-EPCAM**. Despite some **Fe_3O_4-NH-RITC/CO-EPCAM** nanoparticles were still found on the cell membranes, larger aggregates of red nanoparticles were observed next to the nuclei at 6 h (Fig. 8b). At 24 h, there was no nanoparticle found on the cell membranes while large aggregates of red nanoparticles were localized near the

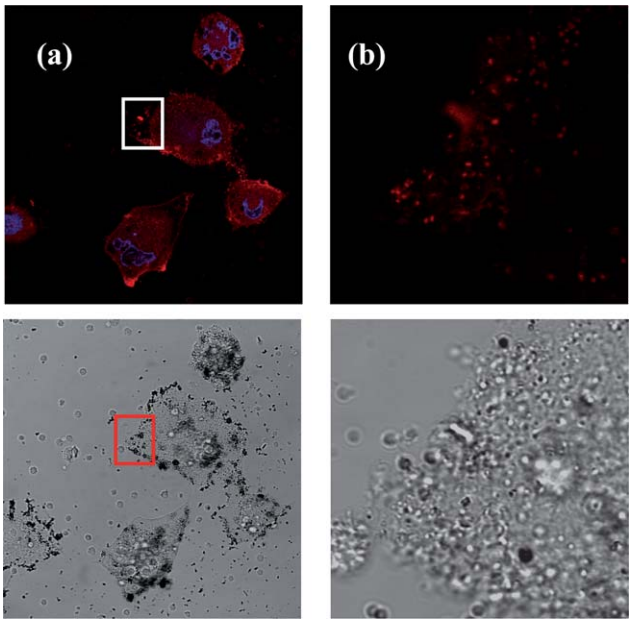

Fig. 9 Confocal fluorescence and bright field microscopy images of Panc-1 cells cultured with **Fe_3O_4-NH-RITC/CO-EPCAM** nanoparticles for 1 h. (a) Middle section of the cells; (b) Magnified images of the inset areas in (a). In blue the cell nuclei stained with DAPI and in red the nanoparticles tagged with RITC.

nuclei. This suggested that all the nanoparticles bound to the EPCAM receptors on the cell membranes were fully internalized in 24 h.

This observation implied that the presence of the EPCAM antibody on the nanoparticles successfully targeted the Panc-1 cells and facilitated their early uptake. For the controls experiments, both **Fe_3O_4-NH-RITC/CO-ISO** and **Fe_3O_4-NH-RITC/COOH** failed to attach to the cells in one hour (Fig. 8d and 8g). However, by 6 h, there are some **Fe_3O_4-NH-RITC/CO-ISO** nanoparticles (Fig. 8e) found on the cell membranes while a small amount of **Fe_3O_4-NH-RITC/COOH** nanoparticles (Fig. 8h) were aggregated near the nuclei. After 24 h, the cells started to internalize nanoparticles regardless of their surface functionality as all three nanoparticle samples were aggregated near the nuclei. These control nanoparticles are thought to be internalized through non-specific endocytosis processes.[57]

It is clear that the antibody-functionalized **Fe_3O_4-NH-RITC/CO-EPCAM** particles have enhanced interaction with the Panc-1 cells compared with the controls, leading to earlier and increased levels of nanoparticle delivery to these cells. However it is also evident, that nanoparticles, regardless of their surface functionalization, will be internalized by the cells with time. On the other hand, the targeting antibody offers both delivery of larger amount of nanoparticle as well as a faster kinetic of delivery (within 1 h instead of 6 h for controls) which may be advantageous. Under natural conditions tumours would need contact with chemotherapeutic agents for some time, either continuously or as bolus injection before an effect is seen. Although it is not shown here, a combination of multiple targeting ligands or application of an external magnetic field used in conjunction with the targeting antibody may accomplish the panacea of tumour identification and destruction. The siloxane

grafting and subsequent chemistry used here allows the assembly of a bifunctional surface of contrasting chemical properties on a magnetic nanoparticle. This platform can be applied to the synthesis of other multifunctional biosystems beyond biomedical diagnosis.

Conclusions

A simple two-step covalent grafting process with functional silanes on iron oxide nanoparticles leads to a bifunctional surface. These nanoparticles possess both amine and carboxylic acid functional groups, and are non-cytotoxic at a concentration below 125 μg mL^{-1}. The combination of these groups enables the covalent binding of two specific functionalities; fluorescent molecules for imaging capability and antibodies for targeting purpose. **Fe_3O_4-NH-RITC/CO-EPCAM** was demonstrated to be able to target epithelial specific EPCAM receptors on the Panc-1 pancreatic cancer cell lines in one hour and initiated a fast internalization of nanoparticles. However, non-specific internalization was observed after 6 h but for a lower quantity of nanoparticles. More importantly this robust, universal protocol can be adapted for attaching other targeting ligands onto the magnetic nanoparticles without a polymer shell, which will allow targeting of other surface receptors that have a known marker. It was shown that the fluorescence imaging and targeting capability of these bifunctional nanoparticles can be further complimented by the MRI contrasting property through the Fe_3O_4 core. As expected the functionalized nanoparticles influence the signal intensity on T_2 weighted images as a function of iron concentration. Multifunctional nanomaterials of this type are likely to have advanced applications in cancer diagnosis due to their bi-/multi-modular imaging capacity. In terms of therapeutic capability, this could be achieved by either attaching a third functional group on surface for delivery of anti-cancer agents or by magnetic hyperthermia exploiting the Fe_3O_4 cores.[58] Moreover, this could also be aided by the possibility of dual magnetic/antibody targeting for tumours. The potentials of these multifunctional nanoparticles could give some much needed advantages over conventional diagnostic methods and therapies for cancers.

Experimental section

Materials

Iron (II, III) oxide nanoparticles (Nanopowder, 20–30 nm, 98%) were purchased from Alfa Aesar. Succinic anhydride (≥ 99%), N,N-dimethylformamide anhydrous (DMF, 99.8%), dimethyl sulfoxide (DMSO, ≥99.9%), tris(hydroxymethyl)aminomethane (TRIS, ≥99.9%), rhodamine B isothiocyanate (RITC), fluorescein 5(6)-isothiocyanate (FITC), *N*-(3-dimethylaminopropyl)-*N*′-ethylcarbodiimide hydrochloride (EDC, ≥ 99%), *N*-hydroxysulfosuccinimide (NHS, ≥ 98.5%), sodium bicarbonate ($NaHCO_3$, 99.5%), sodium carbonate (Na_2CO_3, ≥ 99.5%), 4′,6-diamidino-2-phenyindole (DAPI), phosphate buffer saline tablets (PBS), bovine serum albumin (BSA), anti-rabbit IgG (whole molecule)–FITC antibody produced in goat (FITC-IgG), Bradford reagent and formalin solution neutral buffered (4% PFA) were purchased from Sigma-Aldrich. 3-Aminopropyltriethoxysilane (APTES, 98%) was acquired from Fluorochem. All chemicals were used as received without any further purification. Mouse IgG1 Monoclonal (NCG01) - Isotype Control antibody was purchased from Abcam Plc. Anti Small Cell Carcinoma, epithelial antigen, cl.MOC-31 (EPCAM) was obtained from Monosan. All aqueous solutions were prepared using ultrapure water Milli-Q (Millipore, resistivity 18.2MΩ.cm @25 °C). Bovine serum albumin tagged with FITC was prepared according to literature procedures.[59] Toluene was dried using 4A molecular sieves (Sigma-Aldrich), activated at 300 °C for 3 h.

Grafting of NH_2 groups onto Fe_3O_4 nanoparticles

In a typical experiment, 500 mg of commercial Fe_3O_4 nanoparticles were dispersed in dry toluene (50 mL) using an ultrasonic bath (Fisher Scientific, FB15051, 30–40 kHz) for 10 min under ambient conditions. Subsequently, APTES (0.5 mL, 2.1 mmol) was added dropwise to the nanoparticle suspension and the reaction mixture was refluxed (110 °C) overnight in air using a mechanical stirrer. The nanoparticles were recovered using a NdFeB permanent magnet (Magnet Sales, size: 10 mm diameter and 5 mm height, strength ~1.18 T) and washed 5 times with acetone to remove all traces of unreacted silanes. Finally, the nanoparticles, denoted as **Fe_3O_4-NH_2**, were dried under vacuum for 16 h at room temperature.

Post-functionalization of Fe_3O_4–NH_2 nanoparticles with carboxylic acid groups

Fe_3O_4-NH_2 nanoparticles (200 mg) were suspended in 45 mL of anhydrous DMF under an N_2 atmosphere. Then 30 mg (0.3 mmol) succinic anhydride pre-dissolved in 5 mL anhydrous DMF were added dropwise to the **Fe_3O_4-NH_2** suspension under nitrogen. The resulting mixture was stirred for 24 h at room temperature under nitrogen. The bifunctional **Fe_3O_4-NH_2/COOH** particles were separated from solution using a NdFeB permanent magnet (same specifications as above) and then washed 5 times with acetone in order to remove all traces of DMF and unreacted succinic anhydride. The nanoparticles were dried overnight under vacuum at room temperature.

Characterization of Fe_3O_4-NH_2 and Fe_3O_4-NH_2/COOH nanoparticles

Fourier Transform Infrared Spectroscopy: FTIR spectra were recorded on powder samples on a Bruker Tensor 27 Spectrometer. For each sample, 100 scans in the region from 400 to 4000 cm^{-1} with a resolution of 4 cm^{-1} were accumulated. Thermal gravimetric analysis: TGA was carried out using a TA instrument Q600 thermal balance. Typically 5–10 mg of nanoparticles were heated to 600 °C with 10 °C min^{-1} in air and kept isothermal at 600 °C for 30 min to determine the amount of organic content on the nanoparticles surface. CHN elemental analysis (Thermo EA1112 Flash CHNS-O Analyzer) was also used to analyze the organic content of the functionalized samples. Fluorescent images were acquired using a Leica DM2500 microscope equipped with a Leica DFC350 FX Camera. Confocal microscopy images were obtained with a Leica (SP2 AOBS) microscope. DLS measurements were performed on a Zetasizer Nano ZS from Malvern. MRI images were

acquired using a Bruker Avance III console and gradient system interfaced to a Magnex Scientific 7T, horizontal bore magnet at a ^{1}H resonant frequency of 300 MHz. T_2 was calculated from a set of RARE[60] images acquired with TR = 5000 ms and TE values of 11, 33, 55 and 77 ms.

Fluorescent dye and protein coupling on the bifunctionalized nanoparticles

For fluorescence labelling, 1 mg **Fe_3O_4-NH_2/COOH** nanoparticles were suspended in 0.9 mL 500 mM sodium carbonate buffer at pH 9.5 and 0.1 mL of 0.01% w/v RITC in DMSO was added to the suspension. The reaction mixture was covered with aluminium foil to avoid any photobleaching during the binding process and rotated in a Stuart Rotator SB2, at room temperature overnight. The fluorescently labelled nanoparticles were separated using a permanent magnet and washed with 10 mM Tris-HCl buffer at pH 8.2 until the solution ran clear. Subsequently, the washed nanoparticles were re-suspended in 0.5 mL of 10 mM potassium phosphate buffer with 0.15 M of NaCl at pH 5.5. The sample, denoted as **Fe_3O_4-NH-RITC/COOH**, was stored at 4 °C fully covered with aluminium foil.

For the binding of FITC-BSA onto the **Fe3O4-NH-RITC/COOH** sample, 0.5 mL of activation solution (200 mM EDC and 50 mM NHS) was added to 1 mg of **Fe_3O_4-NH-RITC/COOH** suspended in 0.5 mL potassium phosphate buffer pH 5.5 and the mixture was rotated for 4 h at room temperature. The COOH activated nanoparticles were washed with PBS buffer in order to remove any residual EDC and NHS, and 10 μg FITC-BSA were added to the suspension. The mixture is left to rotate overnight covered with aluminium foil. The unbound FITC-BSA was removed by washing 10 times with PBS buffer. The model antibody molecule (FITC-IgG) was coupled to the **Fe_3O_4-NH-RITC/COOH** nanoparticles using the same protocol.

Cytotoxicity of functionalized nanoparticles

The human pancreatic cancer cell line, Panc-1, was obtained from American Type Culture Collection and maintained in DMEM medium supplemented with 10% fetal calf serum, 2 mM L-glutamine, 2500 I.U./mL penicillin and 5 μg mL^{-1} streptomycin (all from Sigma, Poole, UK) at 37 °C in a humidified atmosphere of 5% CO_2. Cytotoxicity was assessed at 48 h using the EZ4U non-radioactive cell proliferation assay (Biomedica, Vienna, Austria) according to the manufacturer's instructions. In brief, cells were seeded in 96-well plates 5000 cells/well) in medium (100 μL) and grown for 24 h. The medium was then replaced with a fresh portion containing various concentrations of Fe_3O_4 and **Fe_3O_4-NH_2/COOH** (25–500 μg mL^{-1}). Control wells containing only fresh media were also included. Cells were incubated for a further 48 h. Then, 10 μL of MTS reagent was added to each well. Absorbance readings at 450 nm were taken at 3 h following incubation with the MTS reagent. Experiments were performed in triplicate using eight wells for each treatment.

Specific antibody tagging to Fe_3O_4-NH-RITC/COOH particles

For binding antibodies, 100 μg sterile **Fe_3O_4-NH-RITC/COOH** were suspended in 0.5 mL of 10 mM potassium phosphate buffer with 0.15 M of NaCl at pH 5.5. To this suspension 0.5 mL of activation solution (200 mM EDC and 50 mM NHS) was added and the suspension was rotated at room temperature for 4 h. The COOH activated nanoparticles were washed with PBS buffer and 100 μL antibody (EPCAM or non-specific isotype antibody) was added to them. The mixture was rotated overnight covered with aluminium foil. The unconjugated antibodies were removed during repeated washing steps with PBS buffer. The whole binding procedure was carried out inside a class II flowhood. Bradford assay was used to quantify the number of EPCAM antibodies bound onto the nanoparticles. After binding, the antibody concentration of the supernatant was determined as 15.97 μg mL^{-1} using a calibration curve (see SI Figure S5†). This suggests that 7.03 μg mL^{-1} of EPCAM antibodies (or 32.07×10^{12} molecules) were bound onto the nanoparticles. Since, there are 23.7×10^{12} nanoparticles in 1 mg (calculated using the average diameter of a nanoparticle as 25 nm and density of 5.17 g cm^{-3} for Fe_3O_4), it is equivalent to 1.35 EPCAM molecules per NP.

Antibody targeting experiments

Targeting experiments were conducted at 37 °C in 5% CO_2, unless otherwise specified. To determine the targeting abilities and the cellular uptake, 1×10^4 Panc-1 cells were seeded in glassbase dishes (IWAKI 27mm) 24 h prior to the loading with 100 μg mL^{-1} nanoparticles (**Fe_3O_4-NH-RITC/CO-EPCAM**, **Fe_3O_4-NH-RITC/CO-ISO** and **Fe_3O_4-NH-RITC/COOH**) for 1, 6 and 24 h. After the set time interval, cells were then extensively washed with PBS buffer and fixed with 4% paraformaldehyde solution for 20 min. Fixed cells were washed 5 times with PBS and cellular nuclei were stained with 0.5 mL of 2 μg mL^{-1} 4′,6-diamidino-2-phenyindole solution (DAPI).

Statistical analysis

Data were assumed to be non-parametric hence statistical significance testing was performed using the Mann-Whitney U test.[61] A p value of less than 0.05 was considered to be significant. Data were expressed in box and whisker plots and analyzed using Stats Direct™ (version 2.6.2.).

Acknowledgements

The authors thank Ms Karen Davies (Manchester University) for acquiring the MRI data, Dr A. W. M. Simpson for confocal microscopy imaging. This work was supported by the EPSRC (grant numbers EP/H000925 and EP/C511794), a Royal College of Surgeons Pump Prime grant and the Liverpool NIHR Pancreas Biomedical Research Unit.

Notes and references

1 J. Ferlay, D. M. Parkin and E. Steliarova-Foucher, *Eur. J. Cancer*, 2010, **46**, 765.
2 A. Jemal, R. Siegel, E. Ward, Y. P. Hao, J. Q. Xu and M. J. Thun, *Ca-Cancer J. Clin.*, 2009, **59**, 225.
3 O. C. Farokhzad and R. Langer, *ACS Nano*, 2009, **3**, 16.
4 M. De, P. S. Ghosh and V. M. Rotello, *Adv. Mater.*, 2008, **20**, 4225.
5 A. E. Nel, L. Madler, D. Velegol, T. Xia, E. V. M. Hoek, P. Somasundaran, F. Klaessig, V. Castranova and M. Thompson, *Nat. Mater.*, 2009, **8**, 543.
6 H. Wang, R. H. Yang, L. Yang and W. H. Tan, *ACS Nano*, 2009, **3**, 2451.

7 J. Lu, M. Liong, Z. X. Li, J. I. Zink and F. Tamanoi, *Small*, 2010, **6**, 1794.
8 R. Hao, R. J. Xing, Z. C. Xu, Y. L. Hou, S. Gao and S. H. Sun, *Adv. Mater.*, 2010, **22**, 2729.
9 B. Twaites, C. D. Alarcon and C. Alexander, *J. Mater. Chem.*, 2005, **15**, 441.
10 F. M. Kievit, O. Veiseh, C. Fang, N. Bhattarai, D. Lee, R. G. Ellenbogen and M. Q. Zhang, *ACS Nano*, 2010, **4**, 4587.
11 O. V. Salata, *J. Nanobiotechnol.*, 2004, **2**, 1.
12 S. P. Foy, R. L. Manthe, S. T. Foy, S. Dimitrijevic, N. Krishnamurthy and V. Labhasetwar, *ACS Nano*, 2010, **4**, 5217.
13 K. Hayashi, K. Ono, H. Suzuki, M. Sawada, M. Moriya, W. Sakamoto and T. Yogo, *Chem. Mater.*, 2010, **22**, 3768.
14 X. H. Peng, X. M. Qian, H. Mao, A. Y. Wang, Z. Chen, S. M. Nie and D. M. Shin, *Int. J. Nanomed.*, 2008, **3**, 311.
15 C. Fang, O. Veiseh, F. M. Kievit, N. Bhattarai, F. Wang, Z. Stephen, C. Li, D. Lee, R. G. Ellenbogen and M. Q. Zhang, *Nanomedicine*, 2010, **5**, 1357.
16 E. Amstad, S. Zurcher, A. Mashaghi, J. Y. Wong, M. Textor and E. Reimhult, *Small*, 2009, **5**, 1334.
17 G. J. Strijkers, W. J. M. Mulder, G. A. F. van Tilborg and K. Nicolay, *Anti-Cancer Agents Med. Chem.*, 2007, **7**, 291.
18 R. R. Qiao, C. H. Yang and M. Y. Gao, *J. Mater. Chem.*, 2009, **19**, 6274.
19 P. Reimer and B. Tombach, *Eur. Radiol.*, 1998, **8**, 1198.
20 O. Clement, N. Siauve, C. A. Cuenod and G. Frija, *Top. Magn. Reson. Imaging*, 1998, **9**, 167.
21 Y. X. J. Wang, S. M. Hussain and G. P. Krestin, *Eur. Radiol.*, 2001, **11**, 2319.
22 M. K. Yu, Y. Y. Jeong, J. Park, S. Park, J. W. Kim, J. J. Min, K. Kim and S. Jon, *Angew. Chem., Int. Ed.*, 2008, **47**, 5362.
23 A. K. Gupta, R. R. Naregalkar, V. D. Vaidya and M. Gupta, *Nanomedicine*, 2007, **2**, 23.
24 S. L. Chen, F. Reynolds, L. T. Yu, R. Weissleder and L. Josephson, *J. Mater. Chem.*, 2009, **19**, 6387.
25 B. Feng, R. Y. Hong, L. S. Wang, L. Guo, H. Z. Li, J. Ding, Y. Zheng and D. G. Wei, *Colloids Surf., A*, 2008, **328**, 52.
26 A. K. Gupta and S. Wells, *IEEE Trans. NanoBiosci.*, 2004, **3**, 66.
27 M. J. McGuire, J. Addai-Mensah and K. E. Bremmell, *J. Colloid Interface Sci.*, 2006, **299**, 547.
28 M. Chastellain, A. Petri and H. Hofmann, *J. Colloid Interface Sci.*, 2004, **278**, 353.
29 C. C. Berry, S. Wells, S. Charles, G. Aitchison and A. S. G. Curtis, *Biomaterials*, 2004, **25**, 5405.
30 F. M. Kievit, O. Veiseh, N. Bhattarai, C. Fang, J. W. Gunn, D. Lee, R. G. Ellenbogen, J. M. Olson and M. Q. Zhang, *Adv. Funct. Mater.*, 2009, **19**, 2244.
31 M. Takafuji, S. Ide, H. Ihara and Z. Xu, *Chem. Mater.*, 2004, **16**, 1977.
32 E. Strable, J. W. M. Bulte, B. Moskowitz, K. Vivekanandan, M. Allen and T. Douglas, *Chem. Mater.*, 2001, **13**, 2201.
33 M. Mikhaylova, D. K. Kim, C. C. Berry, A. Zagorodni, M. Toprak, A. S. G. Curtis and M. Muhammed, *Chem. Mater.*, 2004, **16**, 2344.
34 A. Jordan, R. Scholz, K. Maier-Hauff, F. K. H. van Landeghem, N. Waldoefner, U. Teichgraeber, J. Pinkernelle, H. Bruhn, F. Neumann and B. Thiesen, *J. Neuro-Oncol.*, 2006, **78**, 7.
35 P. C. Lin, P. H. Chou, S. H. Chen, H. K. Liao, K. Y. Wang, Y. J. Chen and C. C. Lin, *Small*, 2006, **2**, 485.
36 Z. Xu, Q. Liu and J. A. Finch, *Appl. Surf. Sci.*, 1997, **120**, 269.
37 A. Toma, E. Otsuji, Y. Kuriu, K. Okamoto, D. Ichikawa, A. Hagiwara, H. Ito, T. Nishimura and H. Yamagishi, *Br. J. Cancer*, 2005, **93**, 131.
38 R. E. Serda, N. L. Adolphi, M. Bisoffi and L. O. Sillerud, *Mol. Imaging*, 2007, **6**, 277.
39 H. M. Yang, C. W. Park, M. A. Woo, M. I. Kim, Y. M. Jo, H. G. Park and J. D. Kim, *Biomacromolecules*, 2010, **11**, 2866.
40 J. Yang, E. K. Lim, H. J. Lee, J. Park, S. C. Lee, K. Lee, H. G. Yoon, J. S. Suh, Y. M. Huh and S. Haam, *Biomaterials*, 2008, **29**, 2548.
41 P. Zou, Y. K. Yu, Y. A. Wang, Y. Q. Zhong, A. Welton, C. Galban, S. M. Wang and D. X. Sun, *Mol. Pharmaceutics*, 2010, **7**, 1974.
42 S. B. D. Makhluf, R. Abu-Mukh, S. Rubinstein, H. Breitbart and A. Gedanken, *Small*, 2008, **4**, 1453.
43 Y. Zhang, N. Kohler and M. Q. Zhang, *Biomaterials*, 2002, **23**, 1553.
44 K. Cheng, S. Peng, C. J. Xu and S. H. Sun, *J. Am. Chem. Soc.*, 2009, **131**, S1.
45 S. Bruni, F. Cariati, M. Casu, A. Lai, A. Musinu, G. Piccaluga and S. Solinas, *Nanostruct. Mater.*, 1999, **11**, 573.
46 P. J. Launer, in *Infrared Analysis of Organosilicon Compounds: Spectra-Structure correlation. in Silicone Compounds Register and Review*, ed. R. Anderson, B. Arkles and G. L. Larson, Petrarch Systems, Bristol, 4th edn, 1987, pp 100–103.
47 N. Frickel, R. Messing, T. Gelbrich and A. M. Schmidt, *Langmuir*, 2009, **26**, 2839.
48 R. de Palma, S. Peeters, M. J. van Bael, H. Van den Rul, K. Bonroy, W. Laureyn, J. Mullens, G. Borghs and G. Maes, *Chem. Mater.*, 2007, **19**, 1821.
49 J. B. Hall, M. A. Dobrovolskaia, A. K. Patri and S. E. McNeil, *Nanomedicine*, 2007, **2**, 789.
50 G. T. Hermanson, in *Bioconjugate Techniques in Bioconjugate reagents. Zero-length Crosslinkers*, Academic Press, 2nd edn, 2008, pp 215–231.
51 M. R. Pickard and D. M. Chari, *Int. J. Mol. Sci.*, 2010, **11**, 967.
52 G. Malich, B. Markovic and C. Winder, *Toxicology*, 1997, **124**, 179–192.
53 N. Lewinski, V. Colvin and R. Drezek, *Small*, 2008, **4**, 26.
54 A. K. Gupta and M. Gupta, *Biomaterials*, 2005, **26**, 1565.
55 T. R. Pisanic, J. D. Blackwell, V. I. Shubayev, R. R. Finones and S. Jin, *Biomaterials*, 2007, **28**, 2572.
56 D. Fong, M. Steurer, P. Obrist, V. Barbieri, R. Margreiter, A. Amberger, K. Laimer, G. Gastl, A. Tzankov and G. Spizzo, *J. Clin. Pathol.*, 2008, **61**, 31.
57 S. D. Conner and S. L. Schmid, *Nature*, 2003, **422**, 37.
58 P. Wust, U. Gneveckow, M. Johannsen, D. Bohmer, T. Henkel, F. Kahmann, J. Sehouli, R. Felix, J. Ricke and A. Jordan, *Int. J. Hyperthermia*, 2006, **22**, 673.
59 J. M. Goding, *J. Immunol. Methods*, 1976, **13**, 215.
60 J. Hennig, A. Nauerth and H. Friedburg, *Magn. Reson. Med.*, 1986, **3**, 823.
61 M. Harris and G. Taylor, in *Medical Statistics made Easy in Mann-Whitney and Other Non-parametric Tests*, ed. Martin Dunitz, London, 2nd edn, 2003, pp 31–33.